THE DISTINCTIVE SLEEP PATTERN OF THE HUMAN CALCARINE CORTEX: A STEREO-EEG STUDY

Maurizio Gorgoni,[1] Simone Sarasso,[2] Fabio Moroni,[1] Ivana Sartori, [3] Michele Ferrara,[4] Lino Nobili,[5,6] Luigi De Gennaro[1]

[1]*Department of Psychology, "Sapienza" University of Rome, Rome, Italy*

[2]*Department of Biomedical and Clinical Sciences "Luigi Sacco", University of Milan, Milan, Italy*

[3]*C. Munari Center of Epilepsy Surgery, Niguarda Hospital, Milan, Italy*

[4]*Department of Biotechnological and Applied Clinical Sciences, University of L'Aquila, Coppito (L'Aquila), Italy*

[5]*Child Neuropsychiatry Unit, IRCCS, Giannina Gaslini Institute, Genoa, Italy*

[6]*Department of Neuroscience (DINOGMI), University of Genoa, Genoa, Italy*

Corresponding author:

Luigi De Gennaro, Ph.D.

Department of Psychology

University of Rome "Sapienza"

Via dei Marsi, 78; 00185 Roma, Italy.

Tel.: +39-06-49917647

Fax: +39-06-49917508

E-mail: luigi.degennaro@uniroma1.it

Abstract

Study Objectives: The aim of the study was to describe the spontaneous electroencephalographic (EEG) features of sleep in the human calcarine cortex, comparing them with the well-established pattern of the parietal cortex.

Methods: We analysed pre-surgical intracerebral EEG activity in calcarine and parietal cortices during NREM and REM sleep in 7 patients with drug-resistant focal epilepsy. The time course of the EEG spectral power and NREM vs. REM differences were assessed. Sleep spindles were automatically detected. To assess homeostatic dynamics, we considered the 1st vs. 2nd half of the night ratio in the delta frequency range (0.5-4 Hz) and the rise rate of delta activity during the 1st sleep cycle.

Results: While the parietal area showed the classically described NREM and REM sleep hallmarks, the calcarine cortex exhibited a distinctive pattern characterized by: a) the absence of sleep spindles; b) a large similarity between EEG power spectra of NREM and REM; c) reduced signs of homeostatic dynamics, with a decreased delta ratio between the 1st and the 2nd half of the night, a reduced rise rate of delta activity during the 1st NREM sleep cycle, and lack of correlation between these measures.

Conclusions: Besides describing for the first time the peculiar sleep EEG pattern in the human calcarine cortex, our findings provide evidence that different cortical areas may exhibit specific sleep EEG pattern, supporting the view of sleep as a local process and promoting the idea that the functional role of sleep EEG features should be considered at a regional level.

Keywords: Calcarine cortex; Stereo-EEG; Local sleep pattern; EEG power; Sleep spindles

Statement of Significance

In the present study, we assess for the first time the EEG pattern of the human V1 during a whole-night intracerebral recording. We found that the calcarine cortex exhibits a distinctive EEG activity characterized by absence of spindles, overall spectral similarity between NREM and REM sleep, and reduced homeostatic dynamics of NREM delta activity. These findings depict a unique electrophysiological *scenario* further supporting the notion of sleep as a local phenomenon. This is theoretically relevant in that it suggests that the electrophysiological boundaries across different sleep states are not well-defined and has implications for both research (e.g., neural plasticity, cognitive processing, behavioural disconnection, dreaming) and clinical (sleep disorders) domains, for which the observed regional specificity should be carefully considered.

Introduction

Sleep is considered a global behavioural state, which is tightly regulated by central specialized neuronal networks modulating whole-brain activity [1]. Recently, a growing body of evidence revealed local regulatory aspects of sleep [2,3] and suggested that different cerebral areas exhibit specific spatiotemporal sleep electroencephalographic (EEG) patterns [4-7].

Animal studies suggest that the primary visual cortex (V1) is characterized by a peculiar local EEG pattern. The assessment of mice neuronal firing rates points to a lack of homeostatic regulation during sleep in V1 [8], as well as the possible existence of local synaptic strengthening processes during sleep in this area [9,10]. Moreover, a recent study in mice found that primary sensory cortices (including V1), but not associative regions, exhibit slow waves in layer 3 and 4 during REM sleep, possibly accounting for the disconnection from the environment observed in this stage despite the presence of a surface EEG activity close to that observed during wakefulness [11].

Overall, these findings allow to hypothesize the existence of specific sleep EEG features in V1, in relation with local homeostatic processes and mechanisms involved in behavioural disconnection during sleep. At present, however, an exhaustive description of the spontaneous sleep EEG in V1 in humans is still missing. Frauscher and co-workers [12] examined the intracerebral stereo-EEG (SEEG) recordings of the human V1 in epileptic patients, but they limited their analyses to the assessment of possible ponto-geniculo-occipital (PGO) waves comparing tonic and phasic REM sleep. The results showed that V1 was characterized by an increase of sharply contoured theta waves during phasic versus tonic REM sleep, not observed in other brain areas and by decreased delta power during phasic versus tonic REM sleep [12]. More recently, the same group provided an atlas of regional oscillatory activity during human sleep based on intracerebral EEG recordings in a large number of subjects [13]. The authors found a distinct pattern in the mesial occipital lobe, characterized by a dominant theta peak in all sleep stages and a lower number of sleep spindles and slow waves

compared with other brain structures [13]. However, their analyses were limited to brief segments of the first sleep cycle.

The aim of the present study is to assess for the first time the EEG pattern of the human V1 during a whole-night recording, with a particular attention to sleep spindles, slow waves, and homeostatic processes. To this aim, we compared the visual (calcarine) cortex with a cortical area characterized by a well-established sleep pattern: the parietal cortex. We analysed intracerebral SEEG data recorded during sleep of seven epileptic patients without sleep disturbances. Classical features of the EEG power spectra (time course; NREM vs. REM differences) have been measured, and sleep spindles have been automatically detected. Since slow wave activity (SWA) represents a reliable marker of the homeostatic processes underlying sleep need [14], the ratio in NREM delta activity (0.5-4 Hz) between the 1st and 2nd halves of the night and the slope of delta activity during the 1st NREM sleep cycle has been considered to assess, albeit indirectly, mechanisms of homeostatic regulation.

Methods

Subjects

Seven patients (four females, mean age±SE= 27.9±5.9) with drug-resistant focal epilepsy underwent an individualized investigation with stereotactically implanted intracerebral multilead electrodes for an accurate definition of the epileptogenic zone for surgical purposes (see [15] for details on SEEG methodology). Table 1 summarizes patients' demographic and clinical data. The sample includes only those participants whose SEEG revealed that seizures originated outside the structures of interest. The contacts here analysed were free of inter-ictal epileptic discharges and were not involved in the ictal discharge during seizures. Sleep was recorded four days after electrode implantation, so that subjects were adapted to the stereotactic implantation and the procedures for

SEEG recordings. During the study patients maintained the standard doses of anticonvulsant medications (for details see Table 1). The protocol was approved by the Ethical Committee of Niguarda Hospital (ID 939 - 12.12.2013), as part of the presurgical clinical evaluation.

Please insert Table 1 about here

Electrodes placement and EEG/SEEG recordings

SEEG activity was recorded from platinum-iridium semiflexible multilead depth-electrodes, with a diameter of 0.8 mm, 5-18 contacts 2 mm in length and 1.5 mm intercontact distance (Dixi Medical, Besancon, France) [15]. Each patient had two contacts localized unequivocally within the calcarine and parietal cortices (Figure S1). Immediately after the implantation, cone-beam computed tomography was obtained with the O-arm scanner (Medtronic), and registered to preimplantation magnetic resonance imaging (MRI) (voxel size 0.5 × 0.5 × 2 mm). Subsequently, multimodal scenes were built with the 3D Slicer software package [16], and the exact position of leads within the 3D volume of each individual patient was determined using multiplanar reconstructions and Freesurfer [17] computed surfaces. An example of SEEG implantation highlighting the position of a contact located in the calcarine cortex is reported in Figure S2 for a representative patient (#6). The contacts' location in the calcarine cortex was confirmed by visual inspection performed by two neurophysiologists (IS and LN), based on a) presence of lambda waves [18], b) clinical response to low- and high-frequency intracerebral electrical stimulations, with simple and colored visual hallucination, quadrant-specific or central, c) morphology of the visual evoked potentials. Scalp EEG activity was recorded from two platinum needle electrodes placed

during surgery at "10-20" positions Fz and Cz on the scalp. Electroocular (EOG) activity was registered at the outer canthi of both eyes and submental electromyographic (EMG) activity was acquired with electrodes attached to the chin.

EEG and SEEG signals were recorded using a 192-channel recording system (Nihon-Kohden Neurofax-110) with a sampling rate of 1000 Hz. Data were then exported in EEG Nihon-Kohden format and converted into MatLab (MatLab 7.0, The Matworks, Inc.) format using customized routines. We used a bipolar montage between contiguous SEEG contacts and between Fz-Cz scalp EEG electrodes, EOG and EMG derivations. Finally, data were bandpass filtered (0.3-70 Hz), using third order Butterworth filters and downsampled to 200 Hz.

Procedure

The study began at 8 p.m. Patients were connected to the polygraph and the recording started. Then patients were free to decide when going to sleep. The following morning at 7.30 a.m. patients were disconnected and EEG-SEEG data were downloaded from the portable device memory card and stored on the hard disk of a computer.

SEEG data analysis

Sleep was scored in 20 s epochs. EEG recordings were controlled with the aim to remove periods with interictal spikes and pathological EEG signals from the subsequent analysis. No seizures occurred during the selected recordings. Power spectra for the calcarine and parietal derivations were computed by a Fast Fourier Transform routine for 4-s periodograms averaged in 20 s epochs,

separately for NREM and REM sleep. Frequency range was 0.5-30 Hz with one 0.5-Hz bin (0.5-1 Hz) and 29 1-Hz bins (1.1-30 Hz). NREM sleep included stage 2, 3 and 4.

In order to further quantify the differences/similarities between NREM and REM sleep, we also calculated the slope of the Power Spectral Density (PSD) 'background' [19]. The PSD background (i.e., non-oscillatory) is characterized by a decay from slower to faster frequencies [20]. The steepness of such decay is represented by the so-called spectral exponent [19], which has been associated to the balance between excitation and inhibition in neuronal signalling [21], that strongly changes from wake to sleep. Indeed, the EEG spectral exponent is reduced (i.e., exhibits more negative values) in slow-wave sleep compared to wakefulness [20,22,23], while the spectral exponent of REM sleep and wakefulness are substantially similar [20]. Moreover, the PSD of the EEG become steeper as sleep deepens (i.e., from REM sleep, through stage 2, to slow-wave sleep) [24-26]. For these reasons, we also assessed the spectral exponent of the PSD in the calcarine and parietal cortex in NREM and REM sleep.

The PSD background decline approximately according to an inverse power law: PSD(f) ~ $1/f^{\alpha}$ [27]. In the present study, we provide the spectral exponent $\beta = -\alpha$, which represents the equivalent of the slope of a linear regression of the PSD, fit after taking the logarithm of the x and y axis. To avoid a potential bias due to a disproportionate weight of higher-frequencies compared to lower frequency bins in a linear regression [28], we up-sampled the PSD curve with logarithmically spaced frequency bins, resulting in an up-sampled PSD with 4 times the number of data points than the original PSD, providing equally-spaced frequency bins under logarithmic scale. In line with Colombo and coworkers [19], we used a three-steps procedure to estimate the spectral exponent β separately for NREM and REM sleep in both calcarine and parietal derivations: a) a least-square line was initially fit to the PSD, under double-logarithmic axis; b) we considered the frequency bins with large positive residuals (i.e., >1 median absolute deviations of the residual distribution) as likely characterized by oscillatory peaks. The contiguous frequency bins with positive residuals were

considered as part of the base of the peak, and than eliminated from the analysis; c) a final least-square line was fit on the remaining frequency bins, and its slope was considered as the spectral exponent of the PSD background. We avoid to fit the slope for frequencies < 1 Hz, due to the sensitivity of the EEG at these frequencies to slow-drifts of the signal, movement artifacts and high-pass filter-attenuation.

Detection of sleep spindles

Spindles detection was performed following previously published procedures consisting of fully automatic and data-driven routines [29,30]. Presumed spindles were selected based on their power and duration. For each subject, SEEG signals during NREM sleep were band-pass filtered between 10 and 16 Hz (-3 dB at 9.2 and 16.8 Hz) using a 2nd order Chebyshev filter. The instantaneous amplitude of signals was computed via Hilbert transform and two thresholds were defined based on the amplitude time-course. A detection threshold was set at the mean + 4 standard deviation (SD) and amplitude exceeding this threshold were considered putative spindles. Detections within 1 s were merged as single events. A second threshold was set at mean + 1 SD to identify the beginning and the end of spindles and only those events whose duration was between 0.5 s and 2 s were further considered. Among these selected events, only those in which power increases were specific to the spindle range rather than broadband were considered spindles and further analysed. In order to do so, the power of the raw EEG signal going from 1 s before the start to 1 s after the end of a detected event was computed. Only those events with the maximal power value within the spindle range (10-16 Hz) and exceeding 3 SD of the average power across bins were considered real spindles and analysed. Analysed spindle detections were further confirmed by visual inspection performed by one of the authors (M.G.). Spindles falling within the 10-13 Hz frequency range were considered as "slow", while those falling in the 13-16 Hz range were considered as "fast".

Statistical analysis

Time course of EEG frequency bins

An analysis on the time course of SEEG power across sleep periods was performed for each frequency bins. To this aim, for each patient, the total number of epochs pertaining to the first three NREM-REM cycles (i.e., the minimum common number of cycles across patients) were divided into an equal number of intervals (10 equally-spaced steps for each NREM period; 5 equally-spaced steps for each REM period) in order to account for the different durations of the recordings across patients.

Sleep Spindles

Spindle density was calculated as the number of detected spindles divided by artifact-free NREM sleep minutes. The difference in spindle density between calcarine and parietal cortex (for the whole spindle range and separately for fast and slow spindles) was assessed by paired two-tailed *t*-test. Alpha level was set at 0.05.

Comparison between NREM and REM sleep

For both calcarine and parietal cortex, paired two-tailed *t*-tests were performed separately for each frequency bin on log-transformed SEEG power to compare NREM and REM sleep. Because of the large number of comparisons, the False Discovery Rate (FDR) [31] was applied to correct for alpha inflation.

The spectral exponents of NREM and REM sleep were also compared (paired two-tailed *t*-tests) in both calcarine and parietal derivations. Alpha level was set at 0.05.

Measures of homeostatic sleep pressure

1) First versus second halves of the night in NREM sleep

For each subject, the whole night of sleep (i.e., from the sleep onset to the final awakening) has been divided in two halves. The two halves of the night had a comparable number of NREM sleep 20-sec. epochs (1^{st} half: 492.57±115.06 epochs; 2^{st} half: 416.29±80.66; t=1.6; p=0.1). The ratio between 1^{st} and 2^{nd} halves in NREM sleep has been calculated on the spectral power in each derivation separately for each frequency bin. As a reliable index of changes in the homeostatic sleep pressure across the night, the power spectra in the delta band during NREM sleep was calculated as the mean power across frequency bins between 0.5 and 4 Hz. Delta power ratio between the 1^{st} and the 2^{nd} halves was computed and the difference between calcarine and parietal cortices have been assessed by means of paired *t*-test. Alpha level was set at 0.05.

2) Rise rate of delta activity during the first NREM cycle

The rise rate of delta activity (0.5-4 Hz) during the first NREM cycle (i.e., 10 time intervals) was modelled by a linear least-squares regression on individual data, separately for each derivation. The resulting coefficients B (%) were compared between calcarine and parietal cortices by means of a paired two-tailed *t*-test. Alpha level was set at 0.05.

3) Relationship between indices of homeostatic sleep pressure

In order to assess the relationship between the two considered indices of homeostatic sleep pressure, Pearson's correlation coefficient was computed separately between the $1^{st}/2^{nd}$ halves delta activity changes and the rise rate of delta activity during the first NREM sleep cycle. Alpha level was set at 0.05.

Results

Time course of SEEG power during sleep

Figure 1 shows the average time course of log-transformed spectral power in calcarine and parietal cortex during sleep. The parietal derivation exhibited the expected pattern of EEG power, with NREM sleep periods clearly differentiated from REM sleep periods by (a) a higher power in the slowest frequency range (that decreases across the night, pointing to a progressive reduction of the homeostatic sleep pressure), (b) an increase in several bins included in the frequency range that characterize fast sleep spindles range (~12-15 Hz) and (c) a strong reduction in the highest frequencies (>16 Hz).

On the other hand, the calcarine cortex showed a distinctive sleep pattern, characterized by a general similarity between EEG power spectra of NREM and REM sleep that makes difficult to discriminate their time courses at a visual inspection. A descriptive comparison with the parietal derivation suggests that this homogeneity in the calcarine cortex is mainly due to: (a) the absence of difference in the delta power between NREM and REM periods; (b) a low beta power in REM sleep; (c) the absence in NREM of a peak in the spindles frequency range. Moreover, the calcarine cortex did not exhibit the progressive reduction of the slowest frequencies across the NREM cycles during the night.

Please insert Figure 1 about here

Sleep spindles

We found the complete absence of sleep spindles in the calcarine cortex during NREM sleep (Figure 2). Unsurprisingly, the parietal derivation exhibited sleep spindles (mean±SE spindle density: 1.59±0.49), with a higher density for fast (mean±SE: 1.38±0.48) than slow spindles (mean±SE: 0.22±0.09).

Please insert Figure 2 about here

Comparison between NREM and REM

Figure 3 shows the comparisons between NREM and REM sleep EEG power spectra. At a descriptive level (Figure 3a), the power spectra in the two stages were characterized by a marked similarity in the calcarine cortex, at odds with the parietal cortex, and the statistical analysis confirmed this pattern (Figure 3b). In fact, the t-tests performed in the parietal cortex showed a significant (FDR $q \leq 0.036$; $p \leq 0.044$, corresponds to a $t \geq 2.54$) increase between 0.5 Hz and 15 Hz and reduction in the 22-25 Hz frequency range in NREM sleep compared to REM sleep. On the other hand, the t-tests performed in the calcarine cortex revealed a significant decrease at 6 Hz and increase in the 25-29 Hz range in NREM sleep compared to REM sleep. Finally, Figure 3c depicts the results of the comparison between the spectral exponent of the PSD between NREM and REM sleep in the calcarine and parietal derivations. As expected, the parietal cortex exhibited a significantly reduced

spectral exponent (t=9.96; p<0.0001) in NREM (mean±SE: -1.65±0.14) compare to REM sleep (mean±SE: -0.91±0.08), indexing a steeper PSD decay in NREM. On the other hand, the calcarine cortex showed no significant difference (t=0.70; p=0.51) between NREM (mean±SE: -1.68±0.05) and REM sleep (mean±SE: -1.71±0.09).

In a single patient we had the possibility to analyse three minutes of eyes-closed resting wakefulness collected during the morning preceding the sleep recording. With the aim to control (at a descriptive level) if the observed homogeneity of the EEG spectral power in the calcarine cortex is limited to sleep or it is extended to wakefulness, we plotted the EEG power spectra (Figure S3) and the background of the PSD of the EEG decays according to an inverse power-law (Figure S4) of this patient in the calcarine and parietal cortex during eyes-closed resting wakefulness, NREM and REM sleep. Results show that the EEG spectral profile during wakefulness is clearly differentiated from NREM and REM sleep in both calcarine and parietal cortex (Figure S3). Moreover, both the calcarine and the parietal locations exhibit a reduced steepness of the decay of the PSD background during wakefulness, compared to sleep stages (Figure S4).

Please insert Figure 3 about here

Homeostatic sleep pressure

First/second half of the night ratio in NREM sleep

The calcarine cortex exhibited changes of smaller amplitude between 1st and 2nd halves of the night compared to the parietal cortex in NREM sleep, with the latter showing a spectral power decrease under 16 Hz (with higher percentage of change in the slowest frequency bins) and a slight increase in the fastest frequency bins (>16 Hz) in the 2nd half of the night (Figure 4a). Considering the NREM

delta frequency range (Figure 4b), the statistical comparison between the two derivations (t-tests) showed a significantly lower $1^{st}/2^{nd}$ halves ratio (t=2.74; p=0.03) for the calcarine cortex (mean±SE: 116.1±4.35) compared to the parietal cortex (mean±SE: 207.49±33.43).

Please insert Figure 4

Rise rate of delta activity during the first NREM sleep cycle

The calcarine cortex showed a significantly lower rise rate of the delta activity (t=3.17; p=0.02) during the first NREM sleep cycle (mean±SE: 8.17±4.18) compared to the parietal derivation (mean±SE: 38.75±8.93) (Figure 5).

Please insert Figure 5 about here

Correlation between different measures of homeostatic sleep pressure

While the parietal cortex exhibited a significant positive correlation (r=0.76; p=0.04) between the $1^{st}/2^{nd}$ halves of the night changes in NREM delta activity and the rise rate of delta activity during the first sleep cycle, no significant correlation (r=0.18; p=0.70) between these measures of homeostatic sleep pressure has been observed in the calcarine cortex (Figure 6).

Please insert Figure 6 about here

Discussion

Here we provide for the first time an exhaustive description of SEEG activity in the human V1 during sleep. Specifically, using whole-night intracerebral sleep SEEG recordings we found that the calcarine cortex was characterized by: a) the absence of sleep spindles; b) an overall EEG spectral profile similarity and the absence of differences in the spectral exponent of the PSD between NREM and REM sleep; c) signs of reduced homeostatic dynamics, as indicated by the decreased ratio between 1st and 2nd half of the night in NREM sleep and the reduced rise rate of delta activity during the first NREM sleep cycle; d) the absence of correlation between these measures of homeostatic regulation.

Sleep spindles and sigma activity

Taken together, the time course of the EEG activity, the comparison between NREM and REM spectral power, and the automatic spindle detection point to the absence of sleep spindles in the calcarine cortex.

Classically, sleep spindles have been considered as a global phenomenon, highly synchroned across cortical areas [32-34]. However, recent studies pointed to a more local nature of sleep spindles, and our results are in line with these findings [20,30,35-41].

In contrast with our results, sleep spindles have been observed in mouse V1 and lateral geniculate nucleus neurons, and they seem to have a role in cortical plasticity after sensory experience [42]. In humans, sleep spindles have been observed in almost all brain areas studied with intracranial EEG, but their absence in NREM sleep has been previously reported in different locations of the temporal cortex [43]. Nakabayashi and coworkers [43] hypothesized that the lack of spindles in the anterior part of the parahippocampal gyrus could be due to a conserved level of retinal input to the visual cortex in NREM, and to the fact that afferent synaptic drives hindered the intrinsic oscillations in the lateral geniculate nucleus [44,45]. This mechanism could also account for the absence of spindles in the calcarine cortex, given its connections with the lateral geniculate nucleus. Only von Ellenrieder

and co-workers [13] assessed sleep spindles in the human V1 during the first sleep cycle, showing a lower number of spindles in the calcarine cortex compared to other brain structures.

Different thalamocortical pathways target different cortical layers [46,47]. It has been proposed that sleep spindles can be divided in two types depending on the pathway that generate them, with different topographical and laminar distribution [48]. As a consequence, the detection of sleep spindles may be affected by the recorded cortical layer. Beyond replicating our results, future studies should be directly aimed at understanding in what measure the specific layer considered for the recordings can account for the absence of spindles in the calcarine cortex.

Slow wave activity

SWA is a marker of sleep pressure and sleep intensity and is homeostatically regulated. During wake, it increases before sleep onset [49,50] and after sleep deprivation [51,52]; during sleep, it represents a typical feature of the NREM stage, reaching its maximum at the beginning of the sleep period and decreasing progressively during the night [14]. The dynamics of the SWA observed in the parietal cortex in the present study is consistent with this classical description, while the calcarine cortex is characterized by a distinctive SWA pattern. First, we found no SWA difference between NREM and REM sleep. Second, the calcarine cortex exhibited a drastic reduction of two markers of homeostatic sleep dynamics (1^{st} vs. 2^{nd} half ratio and rise rate of the delta frequency during the 1^{st} sleep cycle) compared to the parietal derivation, and the absence of correlation between these measures. In particular, while the calcarine cortex showed a 16.1% greater SWA in the first half of the night compared to the second half, the same comparison for the parietal cortex showed that SWA in the first half was greater by 107.5%.

Previous studies in the calcarine cortex found a reduced delta power during phasic versus tonic human REM sleep [12] and a lower rate of slow waves during N3 in the calcarine cortex compared with the median rate of slow waves among all the channels [13]. Our whole-night results confirm the

existence of a specific modulation of SWA in the calcarine cortex, that points to a) a large power spectra homogeneity across sleep stages and b) the absence of clear overnight homeostatic dynamics.

Recently it has been observed that slow waves occur during REM sleep in layer 3 and 4 of the mouse primary sensory cortices but not associative areas [11]. According to the authors, REM slow waves in primary cortices may account for the sensory disconnection from the environment during this sleep stage despite the presence of a scalp wake-like EEG activity. The absence of differences in the SWA of NREM and REM sleep, then, may represent the expression of a common mechanism of environmental disconnection.

Concerning the homeostatic dynamics of SWA, we propose that the absence of homeostatic SWA changes in the calcarine cortex observed in the present study may indirectly reflect the existence of unusual plastic mechanisms in this area, as also suggested by animal studies. Indeed, Hengen and co-workers [8] found that prolonged monocular deprivation in adolescent mice first induced a reduction of spontaneous firing rates in individual V1 neurons followed by a firing rates recovery to the baseline level during the next 2 days despite continued deprivation. However, this homeostatic recovery of firing rates was enabled only during wake and inhibited during sleep stages. According to the authors, the lack of firing rate homeostasis during sleep suggests that homeostatic plasticity may interfere with sleep-specific processes (e.g., sleep-dependent memory consolidation). Such interpretation argues against the Synaptic Homeostasis Hypothesis, one of the most influent models of the relation between sleep and neural plasticity which claims that the homeostatic regulation of SWA during NREM sleep represents the increase of synaptic strength during wake [53-55]. In another study, firing rates in single V1 neurons were assessed in mice during a period of novel visual experience and in subsequent sleep or sleep deprivation, showing that firing rates increased during post-training sleep and decreased in wake [9]. The authors considered their finding as an evidence of synaptic potentiation during sleep that cannot be easily explained by Synaptic Homeostasis

Hypothesis. Finally, recent findings in mice V1 showed that neuronal firing rates can be increased or reduced during sleep in line with the neurons' baseline activity level [10], supporting the notion that sleep may induce both synaptic strengthening and weakening via spike timing-dependent plasticity [56]. Overall, these data can be better interpreted in light of the hypothesis that sleep may not affect synaptic plasticity in a single way, but it could have different effects influenced by several factors such as the specific cerebral circuit under scrutiny [57], and our results seems to indirectly support this view. Clearly, the interpretation of the present findings in terms of EEG expression of specific local plastic processes in V1 remains speculative, since we did not use any tasks to directly assess use-dependent changes in SWA. Future investigations should be aimed at understanding whether the peculiar SWA pattern observed in the present study represents the EEG expression of a characteristic plastic modulation of the calcarine cortex. Interestingly, several studies found an activation of the occipital cortex in congenitally blind humans after nonvisual sensory inputs [58,59]. Albeit this phenomenon has been usually attributed to a strengthening of cortico-cortical pathways involved in cross-modal plasticity, also presented in the sighted brain, a recent study points to the involvement also of a faster thalamo-cortical connection in this process [60]. According to the authors, such finding raises the question of the specific contributions of thalamo-cortical and cortico-cortical pathways in cross-modal plasticity, and the role of sleep in this processes represents an intriguing issue.

Limitations

Our observation of a large between-stages similarity in the calcarine cortex is limited to the EEG spectral profile and spectral exponent. Such finding does not exclude the possibility that more refined analysis of specific EEG graphoelements pertaining the sleeping calcarine cortex may preserve a certain degree of differentiation between NREM and REM sleep stages. Future investigations should be aimed at assessing this possibility thus confirming/disconfirming our observation above and beyond sheer EEG power analysis.

On the other hand, our results do not allow us to clarify whether the observed between-states power spectra similarity in the calcarine cortex extends also to wakefulness or it is rather limited to sleep. Being a retrospective study, our experimental procedure did not include the systematic analysis of controlled periods of resting wakefulness. Only in one patient we had the opportunity to analyse a period of eyes-closed resting wakefulness, showing that the EEG pattern during wakefulness is clearly differentiated from sleep stages in both calcarine and parietal cortex, and that the decay of the PSD background is less steep during wakefulness, compared to sleep stages, in both regions. Such observation suggests that the homogeneity of the EEG spectral power in the calcarine cortex observed in the present study may be limited to sleep. Future studies should systematically assess this open question.

Conclusions

In the present study we found that the calcarine cortex a) has a substantially uniform EEG spectral profile for both NREM and REM sleep, also showing no differences between sleep stages concerning the spectral exponent of the PSD, b) does not produce sleep spindles, c) does not show clear signs of overnight homeostatic SWA dynamics. To the best of our knowledge, this is the first exhaustive description of the EEG pattern in the human calcarine cortex during an entire night of sleep, and depicts a singular *scenario* in which many well-established assumptions about sleep EEG seem to be questioned, highlighting that sleep involves a complex system of local brain processes. Future efforts should be focused to the assessment of the functional meaning of the local EEG pattern in V1, studying the role of the observed sleep features in neural plasticity and environmental disconnection.

Our findings support the view of a local regulation of sleep [2,3], suggesting that the boundaries between the EEG correlates of different sleep stages are not well-defined, and that their regional specificity should always be considered for clinical and research purposes.

Funding

This work was supported by a grant from Sapienza University of Rome, Avvio alla Ricerca 2018 (AR218164219C41BE) to MG.

Disclosure Statement

Financial disclosure: None.

Non-Financial disclosure: None.

References

1. Moruzzi G, Magoun HW. Brain stem reticular formation and activation of the EEG. Electroencephalogr Clin Neurophysiol. 1949; 1: 455–473.
2. Krueger JM, Nguyen JT, Dykstra-Aiello CJ, Taishi P. Local sleep. Sleep Med Rev. 2019; 43: 14–21. DOI: 10.1016/j.smrv.2018.10.001.
3. Krueger JM, Rector DM, Roy S, Van Dongen HPA, Belenky G, Panksepp J. Sleep as a fundamental property of neuronal assemblies. Nat Rev Neurosci. 2008; 9(12): 910-919.
4. Ferrara M, De Gennaro L. Going local: insights from EEG and stereo-EEG studies of the human sleep-wake cycle. Curr Top Med Chem. 2011; 11: 2423–2427.
5. Sarasso S, Pigorini A, Proserpio P, Gibbs SA, Massimini M, Nobili L. Fluid boundaries between wake and sleep: experimental evidence from stereo-EEG recordings. Arch Ital Biol. 2014*a*; 152: 169–177.
6. Siclari F, Tononi G. Local aspects of sleep and wakefulness. Curr Opin Neurobiol. 2017; 44: 222–227.
7. Gorgoni M, D'Atri A, Scarpelli S, Ferrara M, De Gennaro L. The electroencephalographic features of the sleep onset process and their experimental manipulation with sleep deprivation and transcranial electrical stimulation protocols. Neurosci Biobehav Rev. 2020; 114: 25-37.
8. Hengen KB, Pacheco AT, McGregor JN, Van Hooser SD, Turrigiano GG. Neuronal firing rate homeostasis is inhibited by sleep and promoted by wake. Cell. 2016; 165(1): 180–191.
9. Durkin J, Aton SJ. Sleep-dependent potentiation in the visual system is at odds with the synaptic homeostasis hypothesis. Sleep. 2016; 39(1): 155–159.

10. Clawson BC, Durkin J, Suresh AK, Pickup EJ, Broussard CG, Aton AJ. Sleep promotes, and sleep loss inhibits, selective changes in firing rate, response properties and functional connectivity of primary visual cortex neurons. Front Syst Neurosci. 2018; 12: 40. DOI: 10.3389/fnsys.2018.00040
11. Funk CM, Honjoh S, Rodriguez AV, Cirelli C, Tononi G. Local slow waves in superficial layers of primary cortical areas during REM sleep. Curr Biol. 2016; 26(3): 396-403. DOI:10.1016/j.cub.2015.11.062
12. Frauscher B, Joshi S, von Ellenrieder N, Nguyen DK, Dubeau F, Gotman J. Sharply contoured theta waves are the human correlate of ponto-geniculo-occipital waves in the primary visual cortex. Clin Neurophysiol. 2018; 129(8): 1526-1533.
13. von Ellenrieder N, Gotman J, Zelmann R, et al. How the human brain sleeps: Direct cortical recordings of normal brain activity. Ann Neurol. 2020; 87(2): 289-301.
14. Achermann P, Borbély AA. Mathematical models of sleep regulation. Front Biosci. 2003; 8: s683–s693.
15. Cardinale F, Rizzi M, Vignati E, et al. Stereoelectroencephalography: retrospective analysis of 742 procedures in a single centre. Brain. 2019; 142(9): 2688-2704.
16. Gering DT, Nabavi A, Kikinis R, et al. An integrated visualization system for surgical planning and guidance using image fusion and interventional imaging. In: Medical image computing and computer-assisted intervention – MICCAI'99. Berlin: Heidelberg: Springer; 1999. p. 809–819.
17. Dale AM, Fischl B, Sereno MI. Cortical surface-based analysis: I. Segmentation and surface reconstruction. Neuroimage. 1999; 9: 179–194.
18. Gastaut Y. Un signe électroencéphalographique peu connu: les pointes occipitales survenant pendant l'ouverture des yeux. Rev Neurol. 1951; 84: 640-643.

19. Colombo AC, Napolitani M, Boly M, et al. The spectral exponent of the resting EEG indexes the presence of consciousness during unresponsiveness induced by propofol, zenon, and ketamine. Neuroimage. 2019; 189: 631-644.
20. He BJ, Zempel JM, Snyder AZ, Raichle ME. The temporal structures and functional significance of scale-free brain activity. Neuron. 2010; 66: 353–369. https://doi.org/10.1016/j.neuron.2010.04.020.
21. Gao R, Peterson EJ, Voytek B. Inferring Synaptic Excitation/inhibition Balance from Field Potentials. Neuroimage. 2017; 158: 70–78. https://doi.org/10.1016/J.NEUROIMAGE.2017.06.078.
22. Freeman WJ. Origin, structure, and role of background EEG activity. Part 4: neural frame simulation. Clin Neurophysiol. 2006. 117: 572–589. https://doi.org/10.1016/j.clinph.2005.10.025.
23. Freeman WJ, Zhai J. Simulated Power Spectral Density (PSD) of Background Electrocorticogram (ECoG). Cogn Neurodyn. 2009; 3: 97–103. https://doi.org/10.1007/s11571-008-9064-y.
24. Miskovic V, MacDonald KJ, Rhodes LJ, Cote KA. Changes in EEG Multiscale Entropy and Power-Law Frequency Scaling during the Human Sleep Cycle. Hum Brain Mapp. 2018; https://doi.org/10.1002/hbm.24393.
25. Pereda E, Gamundi A, Rial R, Gonzalez J. Non-linear behaviour of human EEG: fractal exponent versus correlation dimension in awake and sleep stages. Neurosci Lett. 1998; 250: 91–94. https://doi.org/10.1016/S0304-3940(98)00435-2.
26. Shen Y, Olbrich E, Achermann P, Meier PF. Dimensional complexity and spectral properties of the human sleep EEG. Clin Neurophysiol. 2003; 114: 199–209. https://doi.org/10.1016/S1388-2457(02)00338-3.

27. Pritchard WS. The brain in fractal time: 1/f-like power spectrum scaling of the human electroencephalogram. Int J Neurosci. 1992; 66: 119–129. https://doi.org/10.3109/00207459208999796.

28. Hwa RC, Ferree TC. Scaling properties of fluctuations in the human electroencephalogram. Phys Rev E. 2002; 66: 021901. https://doi.org/10.1103/PhysRevE.66.021901.

29. Andrillon T, Nir Y, Staba RJ, et al. Sleep spindles in humans: insights from intracranial EEG and unit recordings. J Neurosci. 2011; 31: 17821–17834.

30. Sarasso S, Proserpio P, Pigorini A, et al. Hippocampal sleep spindles preceding neocortical sleep onset in humans. Neuroimage. 2014*b*; 86: 425-432.

31. Storey JD, Taylor JE, Siegmund D. Strong control, conservative point estimation, and simultaneous conservative consistency of false discovery rates: a unified approach. J Roy Stat Soc Ser B 2004; 66: 187e205.

32. Contreras D, Destexhe A, Sejnowski TJ, Steriade M. Spatiotemporal patterns of spindle oscillations in cortex and thalamus. J Neurosci. 1997; 17: 1179–1196.

33. Achermann P, Borbély AA. Coherence analysis of the human sleep electroencephalogram. Neuroscience. 1998; 85: 1195–1208.

34. Steriade M, Timofeev I. Neuronal plasticity in thalamocortical networks during sleep and waking oscillations. Neuron. 2003; 37: 563–576.

35. Dehghani N, Cash SS, Halgren E. Emergence of synchronous EEG spindles from asynchronous MEG spindles. Hum Brain Mapp. 2011; 32: 2217–2227.

36. Dehghani N, Cash SS, Rossetti AO, Chuan Chen C, Halgren E. Magnetoencephalography demonstrates multiple asynchronous generators during human sleep spindles. J Neurophysiol. 2010; 104: 179–188.

37. Nir Y, Staba R J, Andrillon T, et al. Regional slow waves and spindles in human sleep. Neuron. 2011; 70: 153–169. DOI: 10.1016/j.neuron.2011.02.043

38. Peter-Derex L, Comte J-C, Mauguière F, Salin PA. Density and frequency caudo-rostral gradients of sleep spindles recorded in the human cortex. Sleep. 2012; 35: 69–79.

39. Piantoni G, Halgren E, Cash SS. Spatiotemporal characteristics of sleep spindles depend on cortical location. Neuroimage. 2017; 146: 236-245.

40. Bastuji H, Lamouroux P, Villalba M, Magnin M, Garcia-Larrea L. Local sleep spindles in the human thalamus. J Physiol. 2020; 598(11): 2109-2124. DOI: 10.1113/JP279045

41. Frauscher B, von Ellenrieder N, Dubeau F, Gotman J. Scalp spindles are associated with widespread intracranial activity with unexpectedly low synchrony. Neuroimage. 2015; 105: 1–12.

42. Durkin J, Suresh AK, Colbath J, et al. Cortically coordinated NREM thalamocortical oscillations play an essential, instructive role in visual system plasticity. Proc Natl Acad Sci USA. 2017; 114(39): 10485–10490.

43. Nakabayashi T, Uchida S, Maehara T, et al. Absence of sleep spindles in human medial and basal temporal lobes. Psychiatry Clin Neurosci 2001; 55: 57-65.

44. Fourment A, Hirsch JC, Marc ME, Guidet C. Modulation of postsynaptic activities of thalamic lateral geniculate neurons by spontaneous changes in number of retinal inputs in chronic cats. 1. Input-output relations. Neuroscience. 1984; 12: 453-464.

45. Nunez A, Amzica F, Steriade M. Intrinsic and synaptically generated delta (1-4 Hz) rhythms in dorsal lateral geniculate neurons and their modulation by light-induced fast (30-70 Hz) events. Neuroscience. 1992; 51: 269-284.

46. Jones EG. The thalamic matrix and thalamocortical synchrony. Trends Neurosci. 2001; 24(10): 595–601.

47. Jones EG. Viewpoint: the core and matrix of thalamic organization. Neuroscience. 1998; 85(2): 331–345.

48. Piantoni G, Halgren E, Cash SS. The contribution of thalamocortical core and matrix pathways to sleep spindles. Neural Plast. 2016. doi: http://dx.doi.org/10.1155/2016/3024342

49. Marzano C, Moroni F, Gorgoni M, Nobili L, Ferrara M, De Gennaro L. How we fall asleep: regional and temporal differences in electroencephalographic synchronization at sleep onset. Sleep Med. 2013; 14: 1112-1122.

50. Gorgoni M, Bartolacci C, D'Atri A, et al. The Spatiotemporal Pattern of the Human Electroencephalogram at Sleep Onset After a Period of Prolonged Wakefulness. Front Neurosci. 2019; 13: 312. doi:10.3389/fnins.2019.00312.

51. De Gennaro L, Marzano C, Veniero D, et al. Neurophysiological correlates of sleepiness: a combined TMS and EEG study. Neuroimage. 2007; 36: 1277-1287.

52. Gorgoni M, Ferlazzo F, Ferrara M, et al. Topographic electroencephalogram changes associated with psychomotor vigilance task performance after sleep deprivation. Sleep Med. 2014; 15: 1132-1139.

53. Tononi G, Cirelli C. Sleep and synaptic down-selection. Eur J Neurosci. 2019. DOI: https://doi.org/10.1111/ejn.14335.

54. Tononi G, Cirelli C. Sleep and the price of plasticity: from synaptic and cellular homeostasis to memory consolidation and integration. Neuron. 2014; 81: 12-34.

55. Tononi G, Cirelli C. Sleep function and synaptic homeostasis. Sleep Med Rev. 2006; 10: 49-62.

56. Durkin JM, Aton SJ. How Sleep Shapes Thalamocortical Circuit Function in the Visual System. Annu Rev Vis Sci. 2019; 5: 295-315.

57. Frank MG, Cantera R. Sleep, clocks, and synaptic plasticity. Trends Neurosci. 2014; 37(9): 491-501.

58. Kupers R, Ptito M. Compensatory plasticity and cross-modal reorganization following early visual deprivation. Neurosci Biobehav Rev. 2014; 41: 36–52.

59. Voss P, Pike BG, Zatorre RJ. Evidence for both compensatory plastic and disuse atrophy-related neuroanatomical changes in the blind. Brain. 2014; 137: 1224–1240.

60. Müller F., Niso G, Samiee S, Ptito M, Baillet S, Kupers R. A thalamocortical pathway for fast rerouting of tactile information to occipital cortex in congenital blindness. Nat Commun. 2019; 5154. https://doi.org/10.1038/s41467-019-13173-7

Figures legend

Figure 1: Time course of EEG power. Average time course of EEG power in the 0.5-30 Hz frequency range in the calcarine (left panel) and parietal cortex (right panel) across the first 3 NREM-REM sleep cycles. Data are expressed in logarithmic scale and plotted for 1 Hz bins, with the exception of the frequency range from 0.5 to 1 Hz (plotted for a 0.5 Hz bin).

Figure 2: Spindle density. Whole range (10-16 Hz) spindle density in the calcarine and parietal cortex during NREM sleep. The error bar represents the standard error.

Figure 3: EEG spectral power. EEG spectral power in the 0.5-30 Hz frequency range in the calcarine (left column) and parietal cortex (right column) during a night of sleep. **A.** Mean values of the power spectra during NREM (black line) and REM sleep (grey line). Data are expressed in logarithmic scale and plotted for 1 Hz bins, with the exception of the frequency range from 0.5 to 1 Hz (plotted for a 0.5 Hz bin). Error bars represent the standard errors. **B.** Results of *t*-tests (NREM vs. REM) performed on log-transformed EEG power separately for each frequency bin. Data are expressed as *t*-values. Each bar represents a frequency bin. Asterisks indicate statistically significant differences (FDR $q \leq 0.036$; $p \leq 0.044$, corresponds to a $t \geq 2.54$). **C.** Results of the *t*-tests (NREM vs. REM) performed on the spectral exponent of the power spectral density. Dots represent individual values, horizontal lines indicates the mean of each sleep stage. The asterisk indicates a statistically significant difference ($p<0.05$).

Figure 4: Ratio between 1st and 2nd halves of the night during NREM sleep. A. Power spectra of NREM sleep in the 1st half of the night expressed as a percentage of the 2nd half of the night (100%)

in the calcarine (black line) and parietal cortex (grey line). Mean values are plotted in the frequency range 0.5-30 Hz for 1 Hz bins, with the exception of the frequency range from 0.5 to 1 Hz (plotted for a 0.5 Hz bin). Each dot represents a frequency bin. Error bars represent the standard errors. **B.** Power spectra in the delta frequency range of NREM sleep in the 1st half of the night expressed as a percentage of the 2nd half of the night (100%) in the calcarine (black bar) and parietal cortex (grey bar). The delta band was calculated as the mean of the frequency bins between 0.5 and 4 Hz. Error bars represent the standard errors. The asterisk indicates statistically significant difference ($p \leq 0.05$).

Figure 5: Rise rate of delta activity. Rise rate of delta EEG activity (0.5-4 Hz) during the 1st NREM sleep cycle (10 time intervals). Error bars represent the standard errors. The asterisk indicates statistically significant difference ($p \leq 0.05$).

Figure 6: Correlations between measures of homeostatic modulation. Scatterplots of the individual correlations between 1st vs. 2nd half of the night ratio calculated on delta EEG activity (0.5-4 Hz) during NREM sleep and rise rate of delta EEG activity during the 1st NREM sleep cycle in the parietal (upper panel) and calcarine cortex (lower panel).

Table 1: Demographic and clinical information of each patient.

Patient	Gender	Age (years)	Medications (mg/day)	SEEG				
				Hemisphere	Sample lobe	Calcarine cortex	Parietal cortex	Epileptogenic zone
1	M	40	Tegretol 600-400-600 Gardenale 50-0-100 Rivotril 7-7-7	Left	Temporal-parietal-occipital	Calcarine cortex	Precuneus	Temporal cortex
2	M	55	Carbamazepine (800) Primidone (500) Topiramate (100)	Left	Temporal-parietal-occipital	Calcarine cortex	Superior parietal lobule	Temporal cortex
3	F	34	Topiramate (500) Carbamazepine (1000) Valproic acid (1300) Levetiracetam (1500) Fenobarbital (100) Clobazam (20)	Right	Temporal-parietal-occipital	Calcarine cortex	Paracentral lobule	Dorsolateral cortex of the occipito-parietal junction

4	F	16	Carbamazepine (800) Fenitoine (250) Clobazam (10)	Right	Temporal-parietal-occipital	Calcarine cortex	Postcentral gyrus	Superior parietal gyrus and posterior to the paracentral lobule
5	F	15	Oxcarbamazepine (1200) Levetiracetam (1250)	Right	Temporal-parietal-occipital	Cuneus - Calcarine cortex	Superior parietal lobule	Left frontal cortex (after 2° exploration)
6	M	17	Tolep 750 – 0 – 750 mg/die Frisium 10 – 0 – 10 mg/die Keppra 1250 – 0 – 1250 mg/die	Left	Temporal-parietal-occipital	Calcarine cortex	Precuneus	Temporal cortex
7	F	18	Oxcarbamazepine (600) Felbamate (1200) Clonazepam (2)	Right	Temporal-parietal-occipital	Calcarine cortex	Precuneus	Operculo-insulo-temporo-parietal

Abbreviations: F = Female; M = Male; mg = milligrams; SEEG = Stereo-EEG.

Figure 1

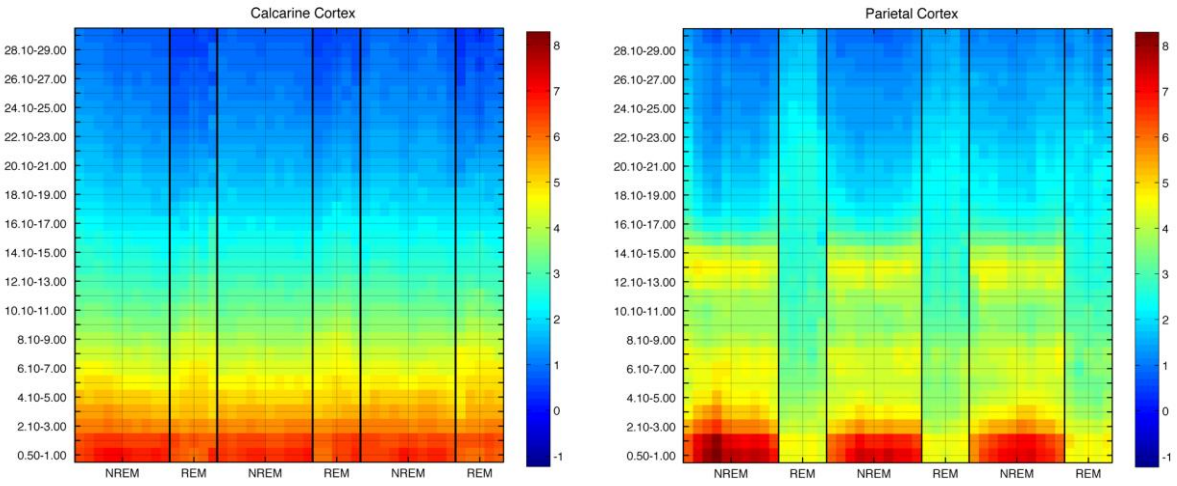

Figure 2

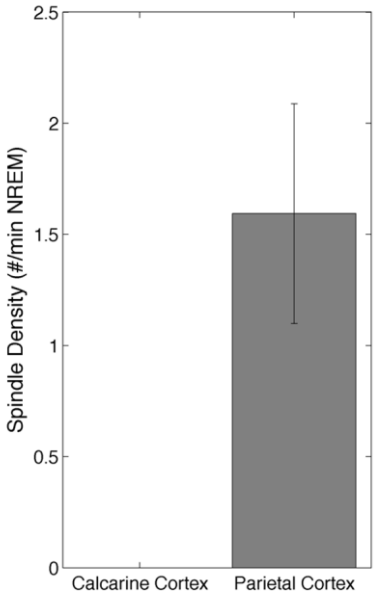

Figure 3

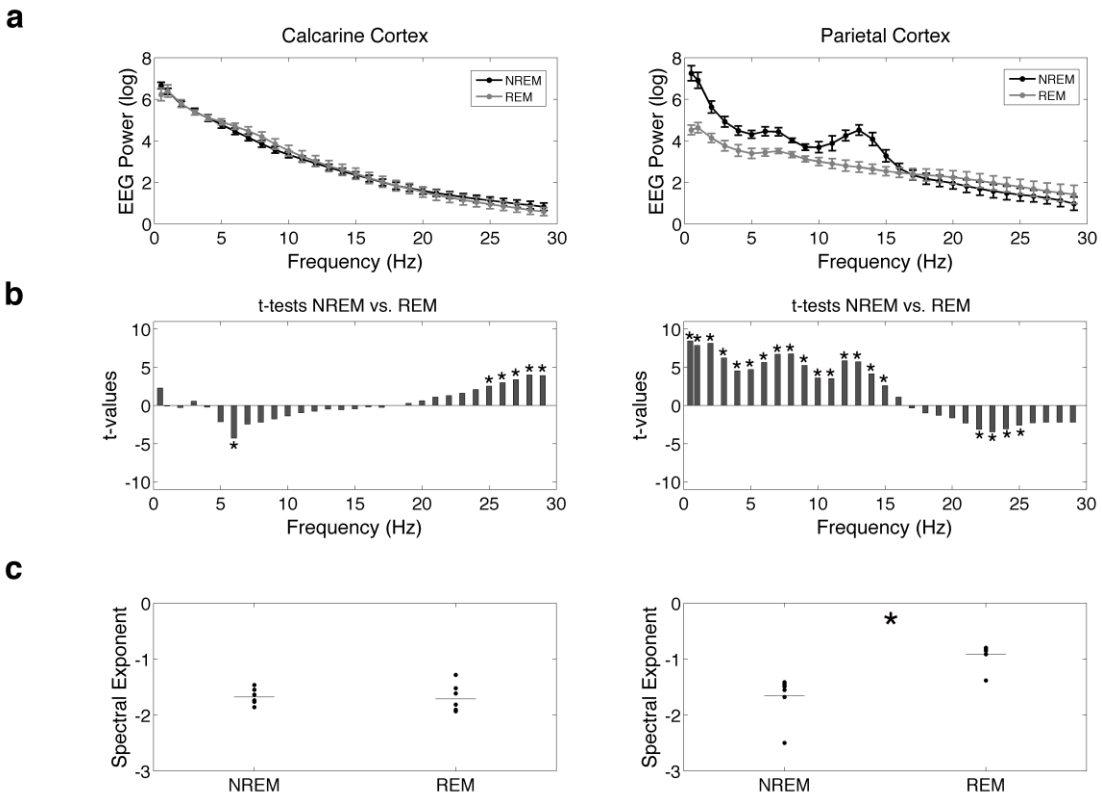

Figure 4

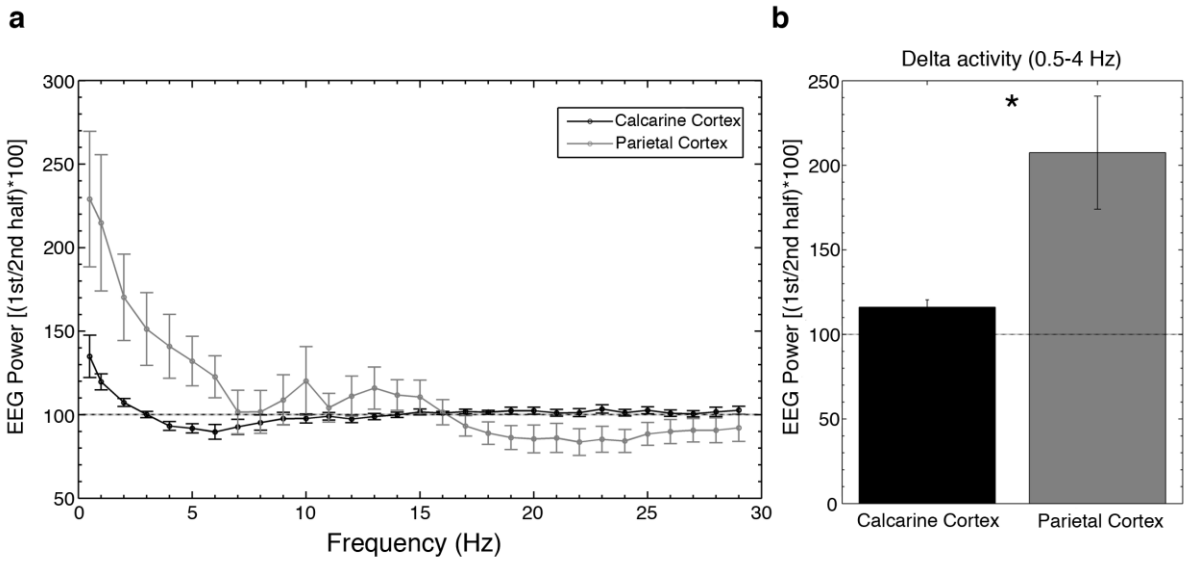

Figure 5

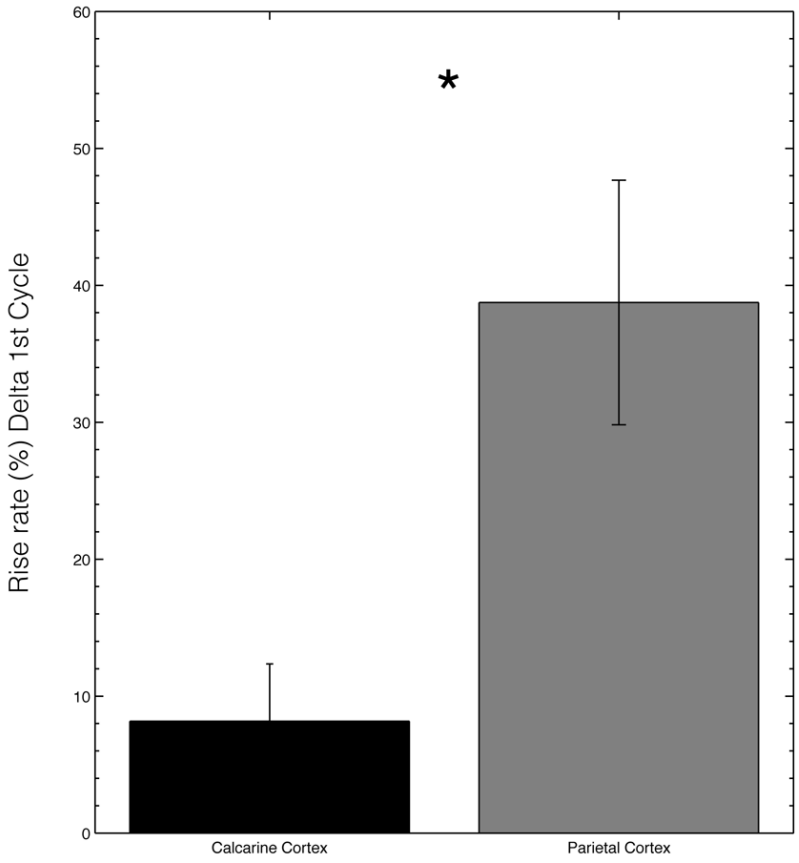

Figure 6